Original Research

Deterministic Lateral Displacement: The Next-Generation CAR T-Cell Processing?

Roberto Campos-González[1], Alison M. Skelley[1], Khushroo Gandhi[1], David W. Inglis[2], James C. Sturm[3], Curt I. Civin[4], and Tony Ward[1] (ORCID)

Abstract

Reliable cell recovery and expansion are fundamental to the successful scale-up of chimeric antigen receptor (CAR) T cells or any therapeutic cell-manufacturing process. Here, we extend our previous work in whole blood by manufacturing a highly parallel deterministic lateral displacement (DLD) device incorporating diamond microposts and moving into processing, for the first time, apheresis blood products. This study demonstrates key metrics of cell recovery (80%) and platelet depletion (87%), and it shows that DLD T-cell preparations have high conversion to the T-central memory phenotype and expand well in culture, resulting in twofold greater central memory cells compared to Ficoll-Hypaque (Ficoll) and direct magnetic approaches. In addition, all samples processed by DLD converted to a majority T-central memory phenotype and did so with less variation, in stark contrast to Ficoll and direct magnetic prepared samples, which had partial conversion among all donors (<50%). This initial comparison of T-cell function infers that cells prepared via DLD may have a desirable bias, generating significant potential benefits for downstream cell processing. DLD processing provides a path to develop a simple closed system that can be automated while simultaneously addressing multiple steps when there is potential for human error, microbial contamination, and other current technical challenges associated with the manufacture of therapeutic cells.

Introduction

The use of a patient's own cells to achieve therapeutic effect dates back to 1956, when E. Donnall Thomas performed the world's first bone marrow transplant to successfully treat a child with leukemia. Since then, significant progress in understanding the immune system and our ability to precisely and effectively engineer synthetic gene constructs has continued to accelerate. Today, it is possible to insert genes that create specific functionality to enable the patient's own immune system, in particular T central memory cells, to effectively target and kill cells that express a particular protein, such as a cell surface tumor marker.[1] These immunotherapy constructs, typically referred to as chimeric antigen receptors (CARs), have shown exceptional promise in treating hematologic cancers, recently winning US Food and Drug Administration (FDA) approval for Kymriah (Novartis) and Yescarta (Kite/Gilead), specifically validating the extraordinary power and efficacy of CAR T-cell approaches in treating B-cell diseases such as B-precursor acute lymphoid leukemia (B-ALL) and B-cell lymphomas. Furthermore, use of CAR T cells is increasingly recognized as a potential approach to treat other hematologic as well as nonhematologic malignancies.[2–5]

Because of continued clinical successes and recent regulatory approvals, progressively higher demand for CAR-T-cell therapy is heightened, putting greater strain on manufacturing approaches that (despite approvals) have documented difficulties with efficiently meeting the prospective demand.[6–8] Targeted gene editing with CRISPR/Cas-9 in focused populations of autologous cells, such as stem cells, potentially might fuel demand even further.[9]

[1]GPB Scientific LLC, Richmond, VA, USA
[2]Department of Engineering, Macquarie University, Sydney, NSW, Australia
[3]Princeton Institute for the Science and Technology of Materials, Department of Electrical Engineering, Princeton University, Princeton, NJ, USA
[4]Center for Stem Cell Biology & Regenerative Medicine and Greenebaum Cancer Center, Departments of Pediatrics and Physiology, University of Maryland School of Medicine, Baltimore, MD, USA

Corresponding Author:
Tony Ward, President, GPB Scientific Cell Processing Division, 800 East Leigh St., Richmond, VA 23219, USA.
Email: tony.ward@gpbscientific.com

Currently, the manufacture of such highly customized autologous therapies is an institutionally focused effort that relies on a labor-intensive process. For example, current CAR T-cell manufacturing processes have between 27 and 32 separate steps, many of which are performed manually.[4,7] Moreover, the automated steps are borrowed or adapted from blood-banking or therapeutic protein-bioprocessing processes, often with room for improvement. Cell losses associated with each individual processing step range from 10 to 35% of cells; in some cases, these processes use chemicals such as ammonium chloride for erythrocyte (RBC) lysis, or stress-inducing hypertonic solutions to achieve cell-specific separations, which sometimes harm cell viability and cause cell losses.[10–14] These losses are generally sustainable in the blood-processing environment for healthy donations or therapeutic apheresis. For cell therapies, however, the donor may be a leukemia patient who is reentering clinical remission after relapse, and has recently been treated with a variety of immunosuppressive agents and standard chemotherapies. As a result, loss of cells at entry into a 3–4-week manufacturing process, coupled with additional cell losses during subsequent steps, is particularly problematic; the process would benefit greatly from having more viable and immunologically responsive cells at every stage of the manufacturing process. At a commercial level, improving cell yields of the desired phenotype (central memory T cells), achieving routine process tolerances and more biological consistency, plus automating each step of the manufacturing process are critical to meet the clinical need for large numbers of therapeutic cells for each patient, and to lower the cost of production of an autologous cell therapy.[1]

The field of microfluidics is rapidly evolving, generating technology for the medical and pharmaceutical industries. These devices often benefit from a closed-system architecture, hands-off operation (once assembled), and high performance—often surpassing what is possible with traditional "benchtop" or hands-on techniques. In addition, microfluidic devices are often constant-flow as opposed to batch processes; as such, the volumes are flexible, and linear scaling is easily achieved via highly parallel design. In the area of label-free cell separation and sorting, multiple approaches achieve high cell purity when isolating a range of targets, including white blood cells, circulating tumor cells, and plasma from whole blood.[15] Of the appropriate methods, only a few are capable of the higher throughput (>mL/min range) necessary to process larger sample volumes without clogging, including deterministic lateral displacement (DLD), spiral inertial separation, straight-channel inertial separation, and centrifugal separations.[16] Our previous research using silicon (Si) and plastic microfluidic chips has shown that DLD microchip-processing technology can provide a solution to automating and speeding up the cell separation process in cell therapy manufacture. DLD microchips harvest cells from a flow of fluid based purely on cell size.[17–19] The DLD approach involves flowing blood through a microchip containing a specifically designed array of microposts that is tilted at a small angle from the direction of the fluid flow. Cells larger than the target size of the micropost array are gently deflected ("bumped") by the microposts into a stream of buffer, effectively separating them from smaller, nondeflected cells and particles, while simultaneously washing the cells in a process that is noninjurious to the cells. In addition to being able to separate by size and wash cells, conscious DLD microchip design allows for concentration of cells using the same principle.[21,22] Salient features of DLD and their potential role in cell processing are described in both **Table 1** and **Figure 1Ai–iii** (and **Suppl. Fig. S1**), which describe the three discrete modes of operation.

In this study, we will focus on apheresis samples, the most challenging category of samples processed by DLD to date, which are integral to CAR T-cell manufacture. The inherent variability associated with donor health, disease status, and prior chemotherapy all affects the quality of the leukapheresis collection, and likely the efficacy of various steps in the manufacturing protocols.[7] To stress test the automated DLD leukocyte enrichment, we collected residual leukocytes (with a leucoreduction system (LRS): leukoreduction chamber fractions) from plateletpheresis donations, which generally have near-normal erythrocyte counts, 10–20-fold higher lymphocytes and monocytes, and almost no granulocytes. They also have ~10-fold higher platelet counts compared to normal peripheral blood. To our knowledge, this is the first instance of using a microfluidic device to separate and purify LRS samples.

We processed 12 donor LRS samples and compared yields of major blood cell types and processivity by DLD versus Ficoll-Hypaque (Ficoll) density gradient centrifugation, which is a gold standard. Furthermore, four of these DLD or Ficoll products were also assessed for activation, subsequent proliferation, and transition to a central memory phenotype. They were also compared to the T-cell expansion capacity of an unpurified aliquot of the donor sample (called a direct magnetic depletion sample, because the sample went directly to the magnetic depletion stage without any upfront purification). These three types of sample (DLD, Ficoll, and direct magnetic product) were stimulated with magnetic beads and processed by magnetic extraction; finally, the product of each magnetic extraction was plated. Time points were chosen at days 3, 8, and 15 to maximally capture upregulation of CD25/interleukin-2 (IL2) before any addition of IL2, and subsequent time points were chosen to effectively capture the IL2-driven expansion and expected conversion to the central memory phenotype by day 14 (**Suppl. Fig. S2**).[23]

Materials and Methods

Microchip Design and Fabrication. The DLD array used in this study consisted of a single-zone, mirrored, diamond post design.[24] There were 14 parallel arrays per chip,

Table 1. Intrinsic Properties of DLD and Their Implications for Cell Processing.

DLD feature	Enablement	Implications
Uniform feature and gap size	Fractionate complex mixtures based on size, with the ability to discriminate particles to within 1–2% in size	Uniform and gentle debulking of platelets and RBC from blood products without centrifugation; up to 99.99% efficiency
		Eliminates open solutions such as Ficoll, and avoids need for harsh or hypertonic solutions (elutriation)
	Ability to sequentially size different cell sizes within the same device	Use of sequential cutoffs to manage highly heterogeneous fractionations
	Cell washing and buffer exchange	Cell washing: >99.9% removal in single pass
		Potential to improve cell culture while maintaining closed system ensuring viable cells
	Concentration	Concentration of cells in culture to make downstream processing seamless
		Minimizes reagent expense without requiring open centrifugation or transfer losses
Deterministic process	Does not rely on random processes such as diffusion	Works better at high speed than slow speed: high throughput
Closeable fluid path	Simple; can be sterilized	Ideal for single use, especially patient-specific therapeutic devices
Low dead volume	<50 µL dead volume per 14-lane microchip	Excellent cell recovery
Requires only positive pressure	Hands-free operation	Potential to automate complex cell-handling and liquid addition exchange processes within a closed system

DLD, Deterministic lateral displacement; RBC, erythrocyte, or red blood cell.

resulting in a 14-lane DLD device (**Fig. 1D**). The device was designed with a 16 µm gap between posts and a 1/42 tilt, resulting in a critical diameter of ~4 µm. The plastic DLD device was generated as described previously from a Si master using a process called soft embossing.[24] Briefly, a micropost design was first fabricated in Si, and then used as a master by casting and curing an elastomer on the surface. This elastomer, once peeled off, had a negative imprint of the Si master (microholes). A plastic sheet was then extruded into the elastomer microholes to create microposts. The elastomer was then peeled off from the plastic device, producing a flat piece of plastic, surface-embossed to a depth of ~100 µm, with a pattern of flow channels and trenches around an array of microposts (**Fig. 1D**, inset). Ports were created for fluidic access to the input and output ends of the microchip. After cleaning by sonication, the device was lidded with a heat-sensitive, hydrophilic adhesive (ARFlow, Adhesives Research, Glen Rock, PA). The overall chip was 40×75 mm in size and 1 mm thick—smaller than the size of a credit card. The microfluidic device was assembled inside an optically transparent, pressure-resistant manifold with fluidic connections. The manifold connected all 14 lanes together such that they could be operated in parallel, using common buffer and sample sources.

DLD Microchip Setup. Silicone tubing (Cole-Parmer, Vernon Hills, IL) was used for all connections to and from the manifold, as shown in **Supplementary Figure S3**. Syringes with locking Teflon caps were used as sealed buffer and sample reservoirs. The closed buffer flow path included a valve at the base of the buffer reservoir to start and stop flow, and an inline degasser (Biotech DEGASi, Minneapolis, MN). The closed sample flow path included a 20 µm PureFlow nylon filter of 25 mm diameter (Clear Solutions, San Clemente, CA) to retain aggregates larger than the microchip's nominal gap size (16 µm), as well as a valve to control flow. The manifold's outlet ports were connected to capped (but at atmospheric pressure) collection reservoirs for the waste and product fractions. Fluids were driven through the DLD microchip using a computer-controlled, constant pneumatic pressure source (MFCS-EZ, Fluigent, Lowell, MA). Two separate pressure controls were used, one for buffer and one for sample.

Prior to loading the sample, the microchip setup was primed and blocked; the protocol followed was previously published and is shown schematically in **Supplementary Figure S3**.[24] Briefly, priming relies on the computer-controlled pressure and on valves and vents to direct flow and flush all air from the tubing, manifold, and chip (~ 5 min); next, the flow is continued for an additional 15 min (hands-off) to fully block all interior surfaces of the closed-path system. At this point, the system is ready to load samples.

Buffer Systems. Three different EDTA-free buffer formulations were tested on the DLD: 0.5% F127 (Pluronic F-127, Sigma Aldrich, St. Louis, MO) in phosphate-buffered saline (PBS) [Ca^{++}/Mg^{++} free] (Quality Biological, Gaithersburg,
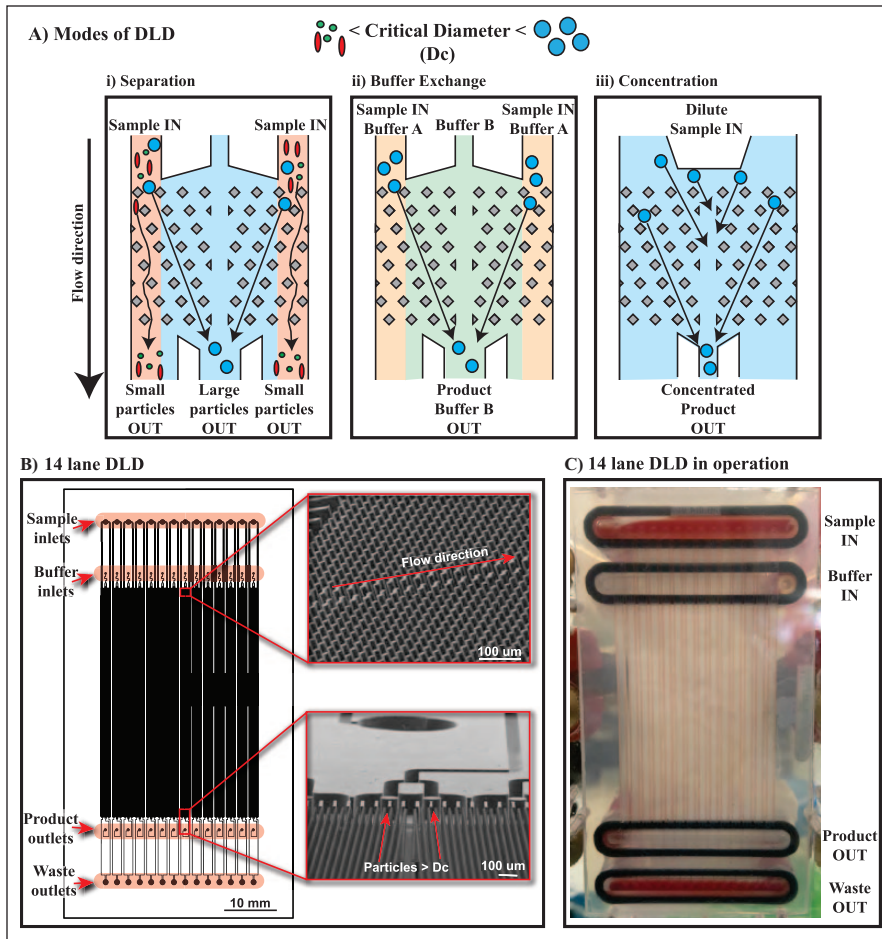
Figure 1. Deterministic lateral displacement (DLD) modes and device used in this study. (A) Operating modes of DLD include (i) separation, (ii) buffer exchange, and (iii) concentration. In each mode, essentially all particles larger than a critical diameter are deflected gently in the direction of the array from the point of entry, resulting in size selection, buffer exchange, or concentration as a function of the geometry of the device. In all cases, particles smaller than the critical diameter pass directly through the device under laminar flow conditions and subsequently off the device. (B) 14-lane DLD design used in separation mode for this project. The full length of the array and microchannel is 75 mm, and the width is 40 mm; each individual lane is 1.8 mm wide. Enlarged scanning electron microscopy (SEM) views of the plastic diamond post array or consolidating collection ports for the exits. (C) Photo of a leukapheresis product being processed using the prototype device at 10 PSI.

MD), 1% bovine serum albumin (BSA) (Affymetrix, Santa Clara, CA) in PBS [Ca^{++}/Mg^{++} free], and an isotonic elutriation buffer (EB) composed of 50% Plasmalyte A (Baxter, Deerfield, IL) and 50% of a mixture containing 1.0% BSA (Affymetrix, Santa Clara, CA) 1.0 mM N-acetyl-cysteine, 2% dextrose, and 0.45% NaCl (all from Sigma-Aldrich, St. Louis, MO). The buffers were prepared fresh each day, and they were sterile-filtered through a 0.2 µm filter flask prior to use on the DLD. All samples in the expansion group were processed using the isotonic elutriation buffer to best align with current CAR T-cell manufacturing approaches, even though better DLD performance has been established with the addition of poloxamer.[23]

Biological Samples. LRS chamber samples from plateletpheresis donations of normal screened donors were obtained using a Trima system (Terumo, Tokyo, Japan), collected at the local blood bank from consented and screened donors. Cell counts were done at the time of collection by the blood bank. Counts were verified in our lab, using a Beckman Coulter AcT2 Diff2 clinical blood analyzer, with ranges of 76–313.3×10^3 white blood cells (WBC)/µL and 0.8–4.87×10^6 platelets/µL. All samples were kept overnight at room temperature on an orbital shaker to mimic overnight shipment (Biocotek, China), and then processed the following day (~24 h after collection). For the initial purification stage, each donor sample ($N = 12$) was processed by either DLD or Ficoll. For the T-cell expansion and immunophenotypic studies, either the DLD or Ficoll purification product, or the native apheresis material (i.e., no initial purification, instead direct to magnetic depletion), were then further processed using magnetic extraction ($N = 4$).

WBC Purification by DLD. LRS sample was diluted with 1 part sample to 4 parts running buffer (0.2×) and then loaded into the sample reservoir. The sample source was pressurized, and the sample valve was opened, resulting in both buffer and sample entering their respective ports on the manifold and flowing through the microchip in parallel (see separation mode in **Fig. 1Ai**). The system automatically processed and separated the entire sample volume, outputting two separate streams of fluid containing product or waste. Both WBC product and RBC/PLT (platelet) waste fractions were collected in pre-weighed, capped, sterile, conical 50 mL tubes and weighed after the collection to

determine the volumes collected, ready for dilution into media.

PBMC Purification by Ficoll. Peripheral blood mononuclear cells (PBMCs) were obtained by diluting the LRS sample to 0.5× in RPMI (Sigma-Aldrich. St Louis, MO), layering on top of an equal volume of Ficoll (GE, Pittsburgh, PA) in a 50 mL conical tube, and centrifuging for 35 min with a free-swinging rotor, without brake, at 400×g. After centrifugation, the top layer was discarded, and the interface PBMC fraction was transferred to a new 50 mL tube and brought up to 20 mL in RPMI. PBMCs were washed by centrifugation for 10 min at 400×g, the supernatant was discarded, and the pellet was resuspended with 20 mL of RPMI and washed again at 200×g for 10 min. The supernatant was removed, and the pellet resuspended in full media.

Purification Recovery Calculation. Before and after isolation using the methods described above, the cell counts were determined using a blood cell analyzer (Beckman-Coulter AcT2 Diff2). Recovery percentages were determined by comparing the net input WBC (Volume In × Cell Count) and the net product WBC (Volume Out × Cell Count). Likewise, RBC and platelet depletion percentages were also calculated. T-cell subtypes were determined using the Coulter counter by estimating a standard 65% of the lymphocyte population to be T cells (standard range: 61–85%).[25]

T-Cell Activation and Magnetic Separation. The number of T cells in each sample for the next stage of activation (Ficoll and DLD products, and native apheresis material for the direct magnetic arm) was estimated based on the Coulter counter measurements as described above. In the direct magnetic extraction arm of the T-cell expansion protocol, 0.5 mL of (native, unpurified) LRS sample was diluted to $1×10^7$ T cells/mL and incubated with immunomagnetic CD3/CD28 beads (5.0 µm, washed and equilibrated; Thermo-Fisher, Waltham, MA) for 1 h at a ratio of 3.2:1 beads per T cell. The mixture was then placed against a magnet for 5 min to capture the T cells. The magnetic bead-bound cells were removed, and the supernatant was measured via Coulter counter to determine the remaining cells; this determined the yield of the magnetic extraction process. Based on this yield value, the bead-bound T-cells in the magnetic-positive fraction were then diluted to $0.5×10^6$/mL for culture in full media. A magnetic depletion yield was determined for each donor.

For samples first purified by either DLD or Ficoll, and then taken through stimulation and expansion, the percentage of T cells in each product was estimated based on the yields observed in the direct magnetic arm. CD3-specific beads enabled high-purity isolation of the T-cell subsets, and we assumed that the efficiency of the magnetic extraction and recovery was constant among all separations. The DLD and Ficoll products were diluted to $1×10^7$ T cells/mL and then activated with anti-CD3/CD28 conjugated magnetic beads using a target ratio of 3.2:1 beads per T cell and incubated for 60 min; the activated T cells were then separated by magnetic depletion for 5 min, and unbound cells were removed. The bead-bound T cells were diluted to $0.5×10^6$/mL and cultured further in full media.

Cell Culture and Cell Activation. In addition to each of the stimulated and separated (stim/sep) T-cell preparations put into cell culture, unstimulated cells (controls) were adjusted to $0.5×10^6$ T cells/mL (assuming T cells at 65% of lymphocytes) in complete media [RPMI-1640 + 10% fetal bovine serum (FBS) (Sigma-Aldrich), plus the antibiotics penicillin 100 units/mL and streptomycin 100 µg/mL (Thermo-Fisher)] and plated. All samples were plated in 6-well plates (Corning, Corning, NY) and cultured at 37 °C, 5% CO_2, in a humidified incubator. Individual wells for each condition (unstimulated, stim/sep with IL2, and stim/sep without IL2) were dedicated to each donor and to each time point. This eliminated any possibility of disruption in expansion due to the sampling and then de-beading activity required for reliable counts, particularly at day 3.

After 3 days in culture, recombinant human IL2 (BioLegend, San Diego, CA) was added at 200 IU/mL to all of the wells presented for expansion (stim/sep with IL2). Following cell culture for up to 15 days, beads were removed from cells, and the cells were counted; this process was repeated at each time point. To remove beads, the cells in the well were resuspended by passing the cells through a 5-mL pipette 10 times. Next, the cell suspension was passed throughout a 1 mL pipette 40 times, followed by vigorous pipetting using a 200 µL tip for 1 min. Then the cell suspension was placed on the side of a magnet for 5 min, and the nonmagnetic fraction was transferred to a fresh tube and counted. The number of cells in the culture wells was determined by using a Scepter 2.0 handheld cell counter (Millipore, Billerica, MA) and by flow cytometry.

Flow Cytometry. No-wash absolute counting by flow cytometry was used for CD3+ cell counts at all time points. Initial day 0 counts used TruCount tubes (BD Biosciences, San Jose, CA) to accurately determine the number of T cells in the native apheresis material, the Ficoll and DLD products, and the supernatant from the direct magnetic fraction; this yielded an actual percentage of T cells for each donor (and an accurate measure of the number of T cells that went into each magnetic depletion reaction). Subsequent days used 123count eBeads Counting Beads at 25,000 per sample (Affymetrix, Santa Clara, CA), which were indexed against TruCount tubes as an internal control. 100 µL of a cell suspension was stained with the CD3-FITC, CD25-PE, and CD45-PerCP conjugated antibodies for 30 min in the dark, either in TruCount tubes or with the addition of 123count

eBeads Counting Beads. The cells were then diluted to 250 μL in PBS with a final DRAQ5 DNA dye (Thermo-Fisher) concentration of 1.0 mM. Next, the stained cells were fixed overnight with an additional 250 μL 1.2% p-formaldehyde in PBS. For absolute count cytometry, a minimum of 25,000 events or 2500 bead events were acquired on a BD FACS-Calibur (BD Biosciences) using a fluorescence threshold (CD45-PerCP).

Phenotypic analysis was also performed at all time points, using a seven-color activation/anergy panel consisting of CD3, CD45RA, CD95, CD279, CD25, CD4, and CD8. At day 15, the panel was modified to create a nine-color panel focused on T central memory, which added CD45RO-PECy7 and CD28-PECy5, and substituted CD197/CCR7 PE for CD279/PD1 PE. For multicolor staining, 100 μl of a cell suspension was stained as above, resuspended to 750 μL in PBS and washed by centrifugation at 400×g, and then resuspended in 250 μL of 1.2% p-formaldehyde and fixed overnight; 25,000 events were acquired using a forward-scatter threshold set to include all intact cells on a four-laser BD FACSAria II (BD Biosciences). Fluorescence compensation was performed using reagent capture beads (UltraComp, eBioscience, Thermo-Fisher). Following fluorescence compensation, intact cells were gated on cell singlets, and T cells were identified as CD3 fluorescence positive versus side-scatter parameters. T-cell subset and subsequent antigen expression analysis was performed using non-CD3 parameters. Central memory T cells were identified by using CD45RO versus CCR7 (CD197) double-positive cells that were also double positive for CD28 and CD95. All data analysis was performed using Flowlogic Software (Inivai, Melbourne, Australia).

Immunofluorescence Staining. Cell fractions to be stained were loaded onto polylysine-coated slides for 10 min and fixed for 15 min in 4% p-formaldehyde + 0.05% Triton X-100 in PBS before washing three times in PBS by centrifugation. Slides were incubated with the conjugated primary antibodies CD41-A647 and CD41-FITC (both from BioLegend) for 60 min in the dark and washed three times with PBS before being mounted in slow-fade mounting media containing the DNA stain DAPI (Thermo-Fisher). Slides were viewed with an Etaluma Lumascope 620 fluorescence inverted microscope (Etaluma, Carlsbad, CA). Monoclonal antibodies (mAbs) conjugated to fluorochromes were obtained from BioLegend: CD25-PE, CD25-APC, CD95-FITC, CD45RA-BV605, CD45RO-PECy7, CD197/CCR7 PE, CD279-PE, CD28 PE-Cy5, CD45-PerCP, CD3-FITC, CD3-BV421, CD4-AF700, CD8-APC-AF780, CD61-FITC, CD41-FITC, and CD45-Alexa647. Viability of the WBC obtained by DLD and PBMCs purified by Ficoll was determined by Trypan blue exclusion performed after obtaining the product cells, before plating cells into culture.

Results

DLD Microchip and Ficoll Processing of Apheresis Products

The DLD and Ficoll separation methods were used to process 12 LRS samples obtained from 12 separate normal donors. Of the 12 samples received and processed, 11 samples clustered around a mean of 152.6×10^3/μL WBC and 2.52×10^6/μL platelets (**Fig. 2A** and **2B**). The 12th sample, with 313.3×10^3/ μL WBC and 4.87×10^6/μL platelet counts, can be seen in the scatterplot as a red triangle (**Fig. 2A**). This sample was sufficiently aggregated at the time of processing that it rapidly clogged the 20 μm prefilter and thus did not fully enter the DLD. Microscopic examination of the input sample showed that this sample was full of platelet–WBC aggregates in the size range of 25–50 μm with multiple aggregates observed as large as 250 μm in diameter (**Fig. 2C** and **2D**). Furthermore, both WBC and platelet counts were greater than three standard deviations above the mean WBC and platelet counts. Using the quartile method, this sample was classified as a mild outlier; using the Grubbs test for outliers and an α-level of 0.05, this sample was also classified as an outlier.[26] As a result, this donor was excluded from the study based on extremely high WBC and platelet counts and being too badly agglutinated and damaged.

A representative image of the input material (LRS product diluted to 0.2×) is shown in **Figure 2B**. Typical micrographs of DLD (**Fig. 2E**) and Ficoll (**Fig. 2F**) cell products from the same input donor show significantly lower background platelet levels (CD41-FITC in green) in the DLD compared to Ficoll. Also shown are the respective cell products, as collected in tubes (**Fig. 2G** and **2H**). DLD processing automated the process of removing the WBC from the RBC and platelets, generating one tube for product and one for waste; the average runtime was 13.1 min (with a sample throughput of ~70 mL/h) once the sample and chip were loaded into the instrument (**Table 2** and **Suppl. Table S1**). The Ficoll sample still required further manual processing to pipette the PMBC layer at the operationally defined interface of the plasma layer above and Ficoll layer below (**Fig. 2H**); plus, an additional minimum of two centrifugal washes was required to remove most of the contaminating platelets. The total processing time of the Ficoll was ~90 min.

The purification efficiency of the Ficoll and DLD devices is summarized in **Table 2** and **Supplemental Table S1**. The WBC recovery and RBC and PLT depletion were calculated by comparing total cells into both purification processes versus total cells out, to account for any volume changes and dilutions. Mean cell recoveries of WBC from DLD were ~80%, 16% higher than from Ficoll (64%), and mean platelet depletion via DLD (85%) was superior to that via Ficoll (56%). The PLT–WBC ratio decreased from an average of 18.2±7.5 to 3.6±2.6 for DLD (a ~fivefold reduction), whereas Ficoll only achieved a reduction down to 11.1±6.7
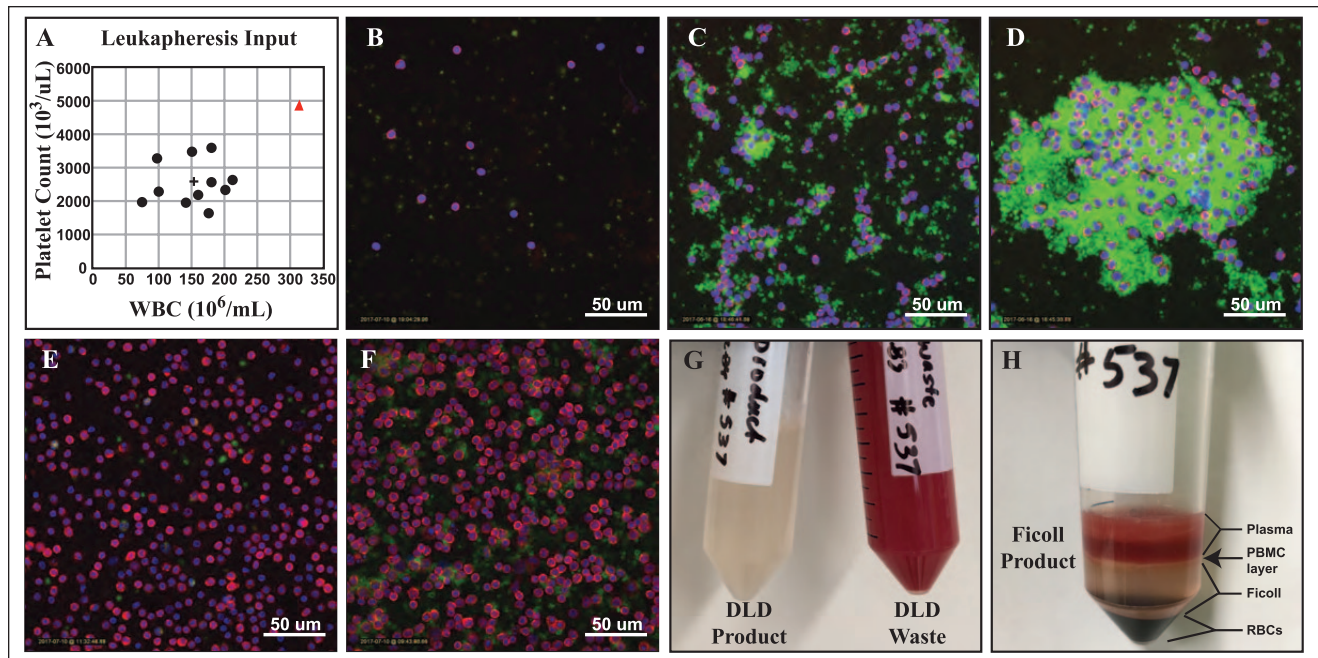
Figure 2. Processing via deterministic lateral displacement (DLD) removes more platelets as compared to Ficoll in parallel leukapheresis samples. (A) Scatterplot showing range of normal donor platelet and white blood cell (WBC) cell counts used in this study. Mean counts: $152.4 \times 10^3/\mu L$ WBC and $2.61 \times 10^6/\mu L$ platelets (+). (B) A typical 24-h-old normal donor leukapheresis input compared with the outlier sample (▲in A, C, and D), which clogged the 20 μm prefilter and was excluded from the dataset. PBMC product processed by either (E) a 14-lane diamond post DLD at 10 PSI or (F) Ficoll. Photograph of (G) representative DLD product and (H) Ficoll from the same leukapheresis donor (donor 37). Input (B–D) and product fractions (E,F) were fixed and stained on slides with CD41-FITC (green platelets) and CD45-Alexa647 (red WBC), and counterstained with DAPI (blue nuclear DNA).

Table 2. Comparison of Purification Efficiency between Ficoll and DLD Devices.

	Input Donor Counts			Purification Efficiency			PLT–WBC Ratios		
	WBC × $10^3/\mu L$	RBC × $10^6/\mu L$	PLT × $10^3/\mu L$	WBC Recovery	RBC Depletion	Platelet Depletion	Donor PLT–WBC Ratio	Product PLT–WBC Ratio	Fold Change PLT–WBC Ratio
Ficoll (N = 11)	153 ± 44	5.3 ± 0.4	2536 ± 652	63.5 ± 16.3%	97.1 ± 1.7%	56.5 ± 22.8%	18.2 ± 7.5	11.1 ± 6.7	1.6
DLD (N = 11)				79.6 ± 13.4%	96.9 ± 1.1%	83.1 ± 12.3%		3.6 ± 2.6	5.1

DLD, Deterministic lateral displacement; PLT, platelet; RBC, erythrocyte, or red blood cell; WBC, white blood cell.

(a 1.6-fold reduction). Mean RBC depletion in these 24-h-old samples was 97% for both DLD and Ficoll, and the average viability of cells obtained by DLD was 96% compared to Ficoll, which was 97%.

T-Cell Isolation and Stimulation

Following DLD or Ficoll purification, T cells were activated using CD3/CD28 magnetic beads for 60 min, separated, and then plated. Due to limited access to a flow cytometer and concerns regarding potential bead interference in product cell counts, we estimated the T-cell count into each reaction as 65% of lymphocytes (normal range: 61–85%). We also counted the input and nonmagnetic fraction (supernatant) of the direct magnetic arm to yield the

number of T cells bound to the magnet by subtraction; this magnetic recovery yield was then assumed for the other two arms of the experiment (Ficoll and DLD), and it was used to determine both an estimate of the correct input bead count (to yield a ratio of 3.2 beads per cell) and also the plating density post magnetic extraction. Accurate T-cell counts were determined post plating into culture using flow cytometry; these counts established the true percentage of T cells for each donor going into each magnetic depletion reaction. This meant that the targeted ratios of 3.2 beads per CD3+ cell, post magnetic separation and as plated, were in fact on average 3.5:1 (3.1–4.2) in the direct magnetic fraction (slightly more beads per T cell than targeted due to low T-cell yield from magnetic depletion), and were on average 2.2 (1.9–2.5) for both the DLD and Ficoll fractions (i.e.,
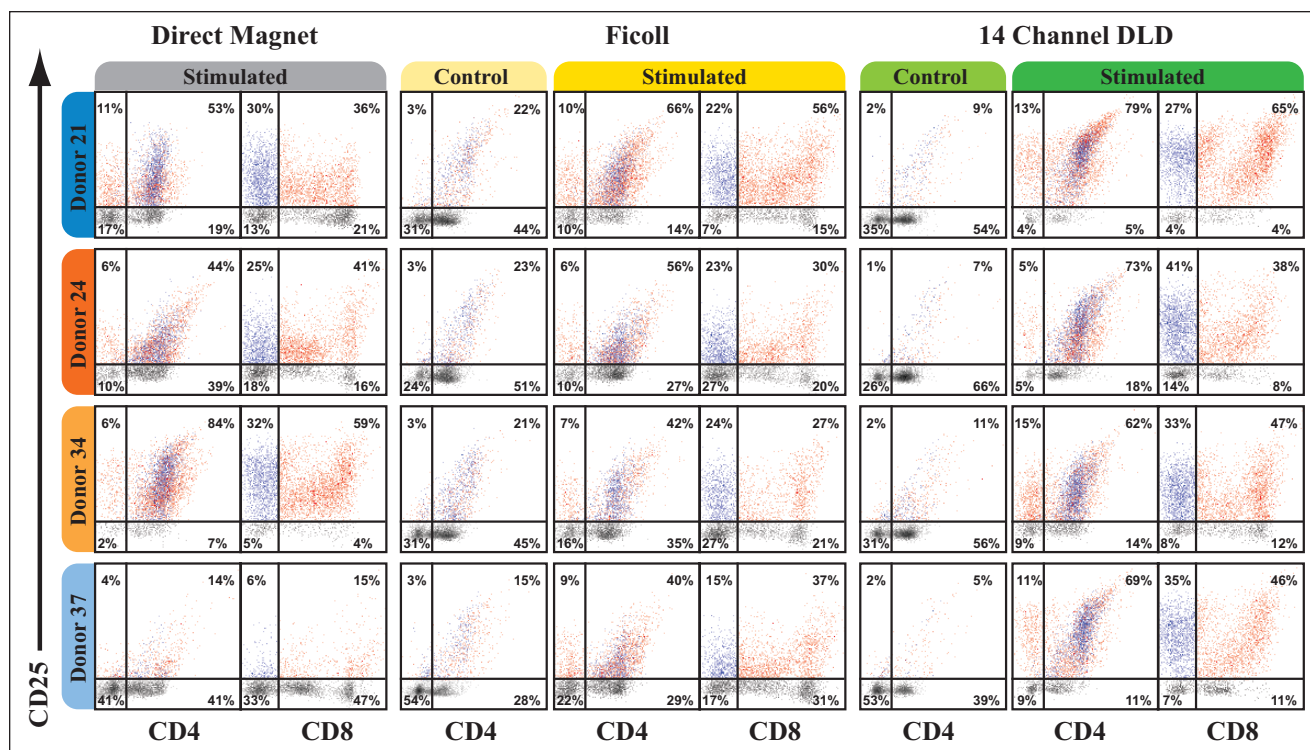
Figure 3. Consistency of cell activation (day 8). Cells were counted and de-beaded, as described previously. At each time point, ~100,000 cells were stained with CD3-BV421, CD45RA-BV605, CD95-FITC, CD279-PE, CD25-APC, CD4-Alexa 700, and CD8-APC-Cy7; incubated for 30 min at room temperature in the dark; and washed with 10 volumes of phosphate-buffered saline (PBS) prior to centrifugation and fixation in 1.0% paraformaldehyde in PBS. Samples were acquired on a BD FACSAria, and they were analyzed using a CD3 and forward- and sidescatter gate using FlowLogic software. Quadrants and markers were set using similarly prepared unstimulated controls (**Suppl. Fig. S4**). Percentages in all plots are rounded.

fewer beads per T cell than targeted, corrected for low yield, and slightly overcompensated based on the actual percentage of T cells of the input sample). T-cell count into the magnetic stimulation step was used as the baseline (day 0) count.

Flow cytometric characterization of the cultures was performed at each time point to assess consistency of cell activation. Changes in CD25 expression of CD3+ cells were measured on day 8 for Ficoll, DLD, and direct magnetic preparations, and they are shown in **Figure 3**. IL2 Receptor-positive (CD25) CD3 cells are shown in blue (CD4+ plots) and red (CD8+ plots). DLD-prepared cells show more consistent phenotypic expression among the four donors for CD25, an indicator of response to CD3/CD28 stimulation, as compared to both Ficoll and direct magnetic preparations. DLD-prepared CD3+ cells had an average 73% response to co-stimulation compared to Ficoll at 51% (both stimulated an average of 2.2 beads/cell), whereas the direct magnetic fraction, stimulated at a higher 3.5 ratio, had only a 54% response. Unstimulated controls for Ficoll and DLD show a marked difference, with DLD-prepared cells remaining CD25 negative in culture compared to Ficoll (**Suppl. Fig. S4**).

In addition to evaluating CD25, conversion to a memory cell phenotype was tracked using the percentage of CD3+ cells that were first activated at day 8 [CD45RA+ (naïve) and CD25+] and then converted toward a central memory phenotype at day 15, indicated by a subsequent loss of the CD45RA+ phenotype as the cells convert to RA− (or antigen-experienced CD45R0+). At day 8, on average, 59% of CD3+ cells were CD45RA− and CD25+ in DLD as compared to 36% in Ficoll and 37% in the direct magnetic arm (**Fig. 4** and **Suppl. Table S2**). These results indicate that a greater percentage of the cultured cells, as generated via DLD, were activated at day 8 compared to cells processed by Ficoll and direct magnetics. In addition, the variability in activation among the four donors was significantly less for the DLD-processed cells compared to cells processed with the other two methods (**Suppl. Table S2**). Once these cells were analyzed at day 15, the DLD-processed cells had lost their CD45RA+ expression as expected, indicating a conversion to the antigen-experienced central memory phenotype. The percentage of CD3 cells that were CD25− and CD45RA− was lowest in the DLD fraction at 12±10.1%, as compared to 33±24.8 and 29±53.4% for Ficoll and direct magnetics, respectively, indicating a more complete,

consistent conversion toward the CD25+ CD45RA− population with the DLD CD3 cells. Cells from donor 34, as processed by a direct magnetic device, showed 49% activation at day 8, but at day 15 they had not yet made the conversion to central memory, still showing 51% CD45RA+. These cells as processed by DLD had 53% activation at day 8, followed by almost a full conversion to central memory at day 15, with only 5% CD45RA+ remaining (**Suppl. Table S2**).

Conversion to the central memory T-cell phenotype was determined on day 15. The phenotyping approach to identifying memory cells used in this study is designed to eliminate any issues with shed antigens such as CD62L.[27] CD3+ cells are gated on a singlet gate followed by a CD3 versus sidescatter; they are then gated in a central memory phenotype using a four-parameter gate consisting of CD95, CD28, CCR7, and CD45R0 (**Fig. 5A**). The population that is (+) for each of those markers is then backgated to display the central memory cells as a percentage of the T cells in culture. The CD4 and CD8 expression profiles of IL2-driven central memory T cells (red) compared to non–central memory T cells (gray) show that there is a slight bias, as expected, toward CD4 given the use of IL2 (**Fig. 5B**). Cells processed via either direct magnetics or Ficoll show distinct expansion of CD8 + non–central memory T cells (gray) as compared to DLD-processed cells, which show more consistent expansion among CD4 and CD8 T-cell subsets. We plotted the percentage of central memory T cells for each donor (**Fig. 5C**), and we set a conversion metric of 50% of the T-cell population being the central memory phenotype; using this metric, the direct magnetic arm achieved only one-third of donors converting, with an average of 48% memory cells and an associated 79% relative standard deviation (RSD). The Ficoll arm was slightly improved, showing 2/4 donors converting, with an average of 47% T central memory cells among all four donors and a 29% RSD. In contrast, the DLD arm showed 100% (4/4) donors achieving central memory conversion, with an average of 74% of T cells converting to the central memory phenotype (average across all four donors) and an RSD among donors of only 13%, indicating more complete and consistent conversion to the desired phenotype.

In addition to the percentage of T central memory cells in culture, the other important metric of comparison is how well the cells expand in culture. The cells from each arm were plated, and the fold expansion of the individual cultures was determined at days 8 and 15 using CD3+ counts, relative to the known number of CD3+ T cells in the magnetic depletion step on day 0. The fold expansion of each donor sample was compared for each method (**Fig. 6A**). Although the direct magnetic approach appears to show higher expansion, the counts are likely significantly affected by the higher bead–cell ratios and corresponding differences in plating density between it and the other two arms of the experiment. Regardless, the donors show significant
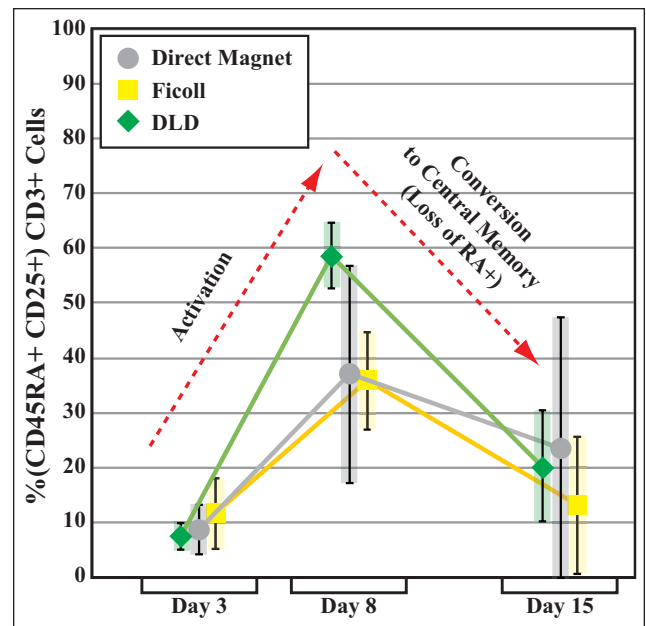

Figure 4. Rapid activation and gain of memory cell phenotype for the four samples processed via deterministic lateral displacement (DLD) compared to Ficoll or direct magnetics. Error bars represent standard deviation of the mean. Plot of percentage of CD45RA− and CD25+ cells shows T-cell activation on day 8 (gain of CD25+ CD45RA+ phenotype) and subsequent conversion to memory cell phenotype on day 15 (conversion to CD45RA−). Cells were fed 200 units IL2/mL culture at days 3 and 8. Raw data are shown in **Supplemental Table 2**.

variability in the fold expansion. In addition, the day 15 culture for direct magnetic arm donor 21 became contaminated and had to be discarded, despite having antibiotics present. It is not possible to know if the day 8 expansion data for donor 21 were influenced by the contaminant.

Comparisons between Ficoll and DLD are valid and much more direct: these cells were stimulated at the same bead–cell ratio and likely had very similar yields from the magnetic extraction due to minimal matrix interference, resulting in almost identical plating ratios. Although the average fold expansion of the DLD cells is not significantly higher than that of the Ficoll cells (13.0 ± 1.1 vs. 11.3 ± 5.5), the consistency of expansion among the set of four donors, and at all days surveyed, is striking.

To obtain the total number of T central memory cells in culture, the WBC recovery from **Table 2**, the fold expansion (**Fig. 6A**), and the percentage of T central memory cells (**Fig. 5C** and **5D**) are multiplied for each donor and for each method (**Suppl. Fig. S2B**). This gives a true end-to-end comparison of the three techniques that takes into account the variable donor T-cell counts, the upfront recovery, and how well these cells expand and convert in culture. On day 15, despite the higher bead–cell ratios in the direct
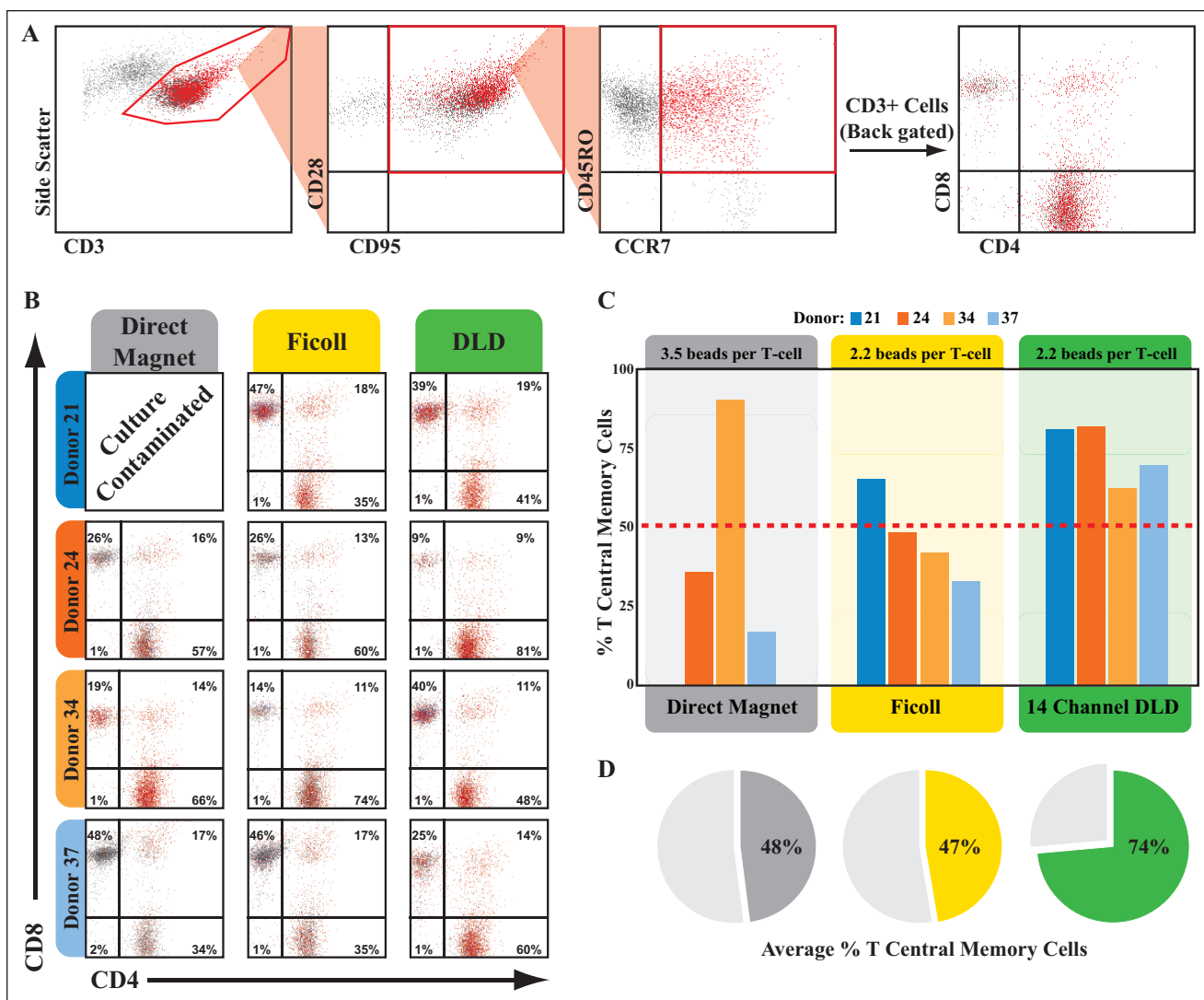
Figure 5. Cytometric analysis of T central memory cells and number of central memory cells produced. (A) CD3+ T cells were gated on a singlet gate, followed by a CD3 versus sidescatter, then followed by central memory phenotyping using four parameter gates of CD28+, CD95+, CD45RO+, and CCR7+ to define the central memory population. The population was backgated to display CD4 and CD8 expression of CD3+ cells, with the central memory cells identified as red. Nonred cells represent all non–central memory T cells. (B) Heterogeneity of CD4 and CD8 expression of T central memory cells (red) and non–central memory T cells among all four donors and three extraction methods. (C) The central memory cells as a fraction of T cells plotted per donor and extraction method shows consistent conversion to the central memory phenotype for cells extracted via deterministic lateral displacement (DLD). (D) The average percentage of T central memory cells is higher for DLD than for Ficoll or direct magnetics.

magnetic arm, on average twice as many memory cells were produced from the DLD arm as compared to either the Ficoll or direct magnetic arms (**Fig. 6B**). The variable T-cell input range (40–123×10^{6}/mL) is reflected in the large standard deviation for each method.

Discussion

In this study, performed at small scale and using parallel testing of the same donors, we demonstrate the suitability and potential advantages of DLD microchips to process

WBC from LRS samples. In our previous work, we demonstrated recovery of 88% of WBC and depletion of 99.98% of RBC from whole blood in a single-lane plastic device designed for small-volume separations.[24] To test the feasibility of DLD for processing leukapheresis samples, and anticipating downstream cell count requirements for culture and stimulation, we moved to a 14-lane format that would process significantly larger volumes, and with a higher volumetric throughput, while minimizing shear forces.[22] We initially investigated processing using the same buffer system as our previous work (F127) and had an average WBC
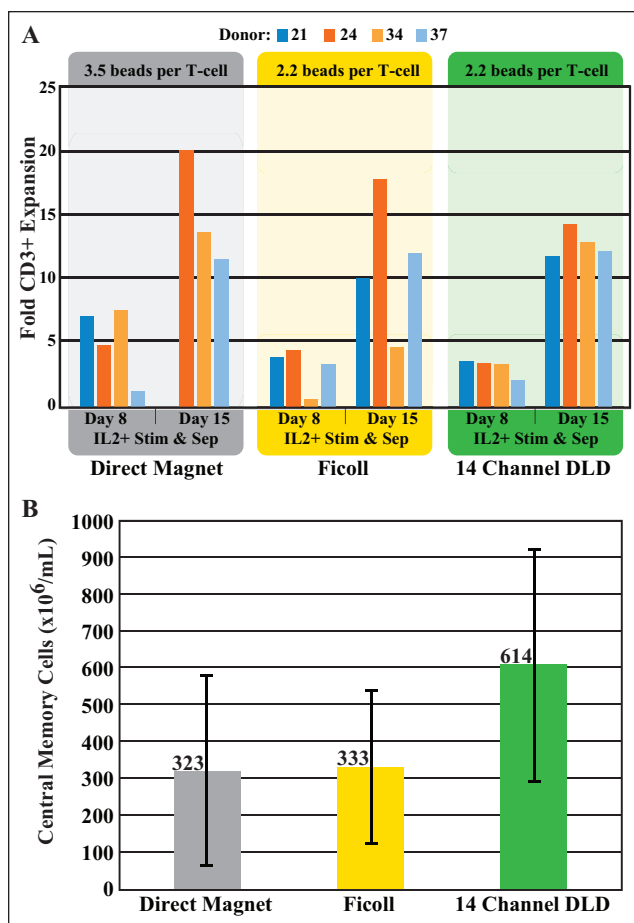
Figure 6. Fold expansion of CD3 and T central memory cells from deterministic lateral displacement (DLD), Ficoll, and direct magnetics. (A) Cell counts were determined on days 8 and 15 (after de-beading) by Coulter count (Scepter, Millipore) and verified by bead-based absolute counting using flow cytometry. Fold expansion of cells processed via DLD was more consistent at 13.0±1.1 [a coefficient of variation (CV) of only 8.6%], compared to 11.3±5.5 (48.3% CV) for Ficoll and 15.2±8.4 (55.4% CV) for direct magnetics. Correlation between counting methods was acceptable with a slope of 0.803, R^2 = 0.792. (B) The donor input T-cell counts, purification step recovery, fold expansion, and percentage of T central memory conversion were cross-multiplied for each method to yield the average net T central memory cells available on day 15.

recovery of >90% from LRS samples, along with RBC and platelet depletion of >96% and >75%, respectively ($N = 4$ of the 11 samples processed; **Suppl. Table 1**). Although these recoveries are in line with our previous results, we instead chose to create an isotonic version of an elutriation buffer used within the blood-banking community because the effects on cell storage, proliferation, stimulation, and phenotype expression are well characterized.[11] Using our closed-chamber, single-pass DLD microchip with a modified blood-banking buffer (without EDTA present), we achieved recovery of 79.6% WBC versus 63.5% by Ficoll.

Our initial goal was to validate the DLD as an alternative to the labor-intensive WBC separation process, one that would provide improved recovery and purity without requiring hands-on skilled labor to complete the separation process. Although the higher yields afforded by DLD were as expected based on our previous studies, the consistency of stimulation and expansion of these cells in culture afforded an unexpected point of contrast between DLD, Ficoll, and direct magnetic extraction (no purification before magnetic stimulation and separation). Specifically, in surveying the phenotypic responses among the four different donors, the DLD product had both a higher and more uniformly consistent CD25+/CD45RA− and CD4+/CD25+ expression, even compared to cells stimulated with a higher bead–cell ratio. The phenotypic analysis of the expanding cells shows the expected shift toward a CD45RA−/CD45RO+ status (**Fig. 4**), and the activation profiles are consistent with cells expanding toward a T central memory phenotype (**Fig. 5** and **Suppl. Figs. S4** and **S5**). At day 15, on average 74% of the CD3+ cells in culture from donors processed via DLD were of the T central memory phenotype, compared to only 48% and 47% for direct magnetics and Ficoll, respectively. In addition, there was significantly less variation within donors for the DLD method, indicating a more consistent phenotypic expression.

Furthermore, DLD processed cells showed more consistency in the rate of expansion, yielding an average 13.0±1.1 (8.6% CV) fold expansion at day 15 versus 11.3±5.4 (48.3% CV) for Ficoll. The direct magnetic expansion was higher as expected due to the greater number of stimulation beads, but the increase was very inconsistent at 15.2±8.4 (55.4% CV). These numbers indicate that, for a standardized input number of T cells in a stimulation and expansion protocol, cells generated via DLD generally expand better and more uniformly compared to cells generated by Ficoll. We multiplied the recovery, phenotypic conversion, and fold expansion to get a net effect of DLD processing versus Ficoll and direct magnetic processing; the yield of T central memory cells was almost twofold higher when the samples were processed via DLD compared to the other methods.

The ability to generate desired cells in a robust and predictable manner is of significant value to both the manufacturing and clinical environments. For the manufacturer, a more predictable and controllable process means that capacity planning and optimization can be taken to new levels; specifically, the ability to generate twice as many cells will require less time in culture (and lower media expense) to generate sufficient cells for dosing. For the clinician and patient, greatly improved predictability will improve the scheduling of conditioning for the patient. Finally, if processing and activation are initiated at the point of collection, there is an opportunity to eliminate the cell loss-inducing steps such as cryopreservation by putting more cells that are healthier into the expansion phase within a few hours of collection.

One potential factor that may explain the greater performance of cells generated via DLD is the degree to which platelets are either removed or still present, whether going into the magnetic stimulation and depletion step or in culture. We hypothesized that platelets, and platelet-derived factors, presented falsely stimulated cells and impeded the correct stimulation pathway once beads were introduced.[28–29] The greater removal of platelets via the DLD process, and the corresponding low activation profile of unstimulated controls (no magnetic depletion, and PLT–WBC ratios as reported in **Table 2**), supports that hypothesis. The platelets may interfere with the cell stimulation and activation process, both preventing T cells from binding to beads and affecting the magnetic extraction yield, but also potentially carrying over into culture and preventing activation and long-term expansion. We see evidence of this in our data: in particular, donor 34 had limited expansion at day 8 and never achieved much expansion at day 15 after processing via Ficoll, whereas that donor expanded as expected (at both days 8 and 15) once processed by DLD. Of note is the high PLT–WBC ratio of the Ficoll sample in culture. Due to the greater efficiency of the DLD separation (WBC recovery and platelet removal), donor 34 had greater purity when processed via DLD (3:1 PLT–WBC for DLD vs. 17:1 for Ficoll in their respective products) and therefore greater purity when input to the stimulation and expansion steps. The direct magnetic extraction was highly variable in both the percentage of T central memory and the fold expansion. Based on our initial measurements of magnetic depletion yield, we know the direct magnetic arm yielded on average 77.6±10.4% depletion of platelets before plating, but the full platelet count was present during the initial bead activation step; the variability may be indicative of the sample quality heading into the stimulation and expansion process.

More complete removal of platelets is a future goal of our research, and the variability of the input donor material that we experienced suggests that upstream improvements to the sample quality (e.g., preventing clumps of platelets that mimic WBC and are bumped, or preventing co-association of platelets and WBC) may yield better results. We previously investigated adding inhibitors at the point of collection to shut down platelet activation pathways, and we demonstrated successful processing of blood from end-stage cancer patients on DLD; a future direction of our research is to investigate how inhibitors at the point of collection, resulting in even greater purity of cells collected from DLD, would affect the downstream proliferation and activation of T cells.[30]

The results shown here not only demonstrate a net greater number of T central memory cells delivered at day 15 compared to via other methods, but also show a process that lends itself more easily to automation. The manual steps required for DLD are significantly fewer (loading
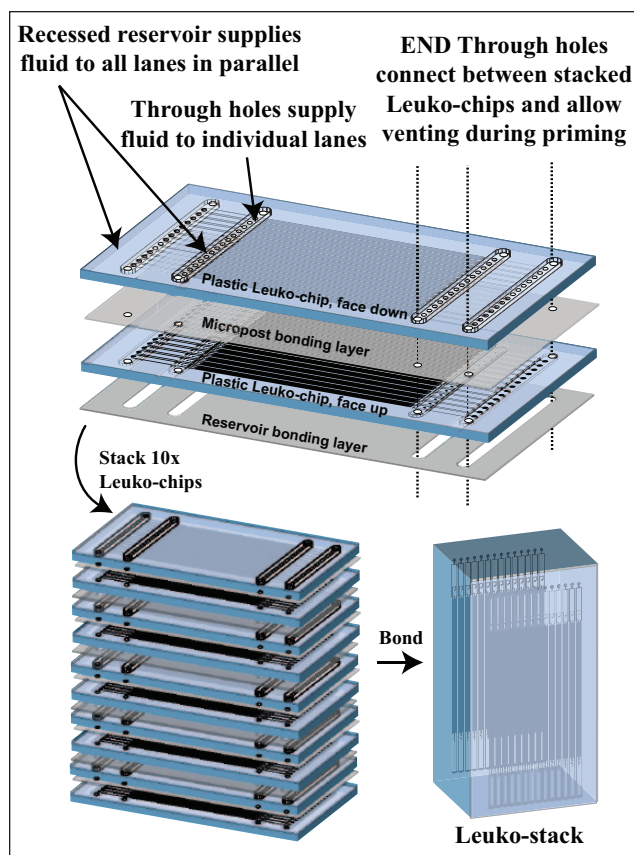

Figure 7. Schematic showing how current individual chips have been designed to be stackable in layers to achieve throughput as demanded by any particular application using established manufacturing approaches. Injection-molded layers are planned as systems are developed.

microchip and sample), and the most critical part, the actual separation, is completely hands-free. Of equal importance is the fact that the T cells expand at a consistent rate once isolated by DLD, and they convert to the central memory cell phenotype at a consistent rate. Processing by DLD removes the variability among donors, potentially allowing a more automated downstream process as well.

With this promising initial data, scaling up and increasing DLD throughput are obvious requirements to achieve processing of leukapheresis samples (200–400 mL). Preliminary designs of our higher throughput modules using the existing 14-lane DLD microchip stacked in multiple layers, along with the necessary interface materials to enable proper distribution of sample and buffer, allow maintaining of suitable form factor (**Fig. 7**). Stacked DLD microchips have been demonstrated previously in Si at Princeton University, and other publications have shown stacking of microfluidic chips, in a range of materials, to enable either parallel processing or increased throughput.[31] Our preliminary work has shown the ability to stack up to six microchips, and we have processed blood on stacks of

2× plastic microchips, recording average WBC recoveries of >80% and depletion of RBC and platelets at >99% and >73%, respectively; furthermore, the throughput scales in a predictable linear fashion. As we transition toward injection-molded modules, we expect stacking microchips will become even more feasible.

In conclusion, DLD has shown that the manual steps performed by a skilled technician in Ficoll preparation can be replaced by easily automated, closed-system DLD. In addition, DLD processing provides other significant benefits, including the recovery of substantially more cells and the ability to generate demonstrably higher quality cells that can be expanded readily and predictably, leading to a more robust and consistent process. Furthermore, the results allude to the potential of DLD-produced cells in conferring a more complete and consistent degree of phenotypic expression, as compared to Ficoll and direct magnetic approaches. Reliable cell recovery and expansion are fundamental to the successful scale-up of any cell therapeutic process; our proposed scaled-up, closed-format, and automatable DLD enables a clear path toward a fully automated closed system, in which an apheresis sample could be prepared and fully processed into the first steps of expansion within 2–3 h of collection, without requiring a skilled tissue culture technician on site.

ORCID iD

Tony Ward 🔟 https://orcid.org/0000-0003-4951-3627

References

1. Berger, C.; Jensen, M. C.; Lansdrop, P. M.; et al. Adoptive Transfer of Effector CD8+ T cells Derived from Central Memory Cells Establishes Persistent T Cell Memory in Primates. *J. Clin. Invest.* **2008**, *118*, 294–305.

2. Vonderheide, R. H.; June, C. H. Engineering T-Cells for Cancer: Our Synthetic Future. *Immunol. Rev.* **2014**, *257*, 7–13.

3. Fousek, K.; Ahmed, N. The Evolution of T-Cell Therapies for Solid Malignancies. *Clin. Cancer Res.* **2015**, *21*, 3384–3392.

4. Wang, X.; Riviere, I. Clinical Manufacturing of CAR-T-Cells: Foundation of a Promising Therapy. *Mol. Ther. Oncolyt.* **2016**, *3*, 16015.

5. Sadelain, M.; Rivière, I.; Riddell, S. Therapeutic T-Cell Engineering. *Nature*, **2017**, *545*, 423–431.

6. National Cell Manufacturing Consortium. *Achieving Large-Scale, Cost-Effective, Reproducible Manufacturing of High Quality Cells: A Technology Roadmap to 2025*. October 2016. https://www.wesrch.com/medical/pdfME1XXF000A-CLN.

7. Levine, B. L.; Miskin, J.; Wonnacott, K.; et al. Global Manufacturing of CAR T-Cell Therapy. *Mol. Ther. Meth. Clin. Dev.* **2017**, *4*, 92–101.

8. Couzin-Frankel, J. Supply of Promising T-Cell Therapy Is Strained. *Science* **2017**, *356*, **1112**.

9. Johnson, L. A.; June, C. H. Driving Gene-Engineered T-Cell Immunotherapy of Cancer. *Cell Res.* **2017**, *27*, 38–58.

10. Hokland, P.; Heron, I. The Isopaque-Ficoll Method Re-evaluated: Selective Loss of Autologous Rosette-Forming Lymphocytes during Isolation of Mononuclear Cells from Human Peripheral Blood. *Scand. J. Immunol.* **1980**, *11*, 353–356.

11. Stroncek, D. F.; Fellowes, V.; Pham, C.; et al. Counter-Flow Elutriation of Clinical Peripheral Blood Mononuclear Cell Concentrates for the Production of Dendritic and T-Cell Therapies. *J. Transl. Med.* **2014**, *12*, 241.

12. Powell, D. J., Jr.; Brennan, A. L.; Zheng, Z.; et al. Efficient Clinical-Scale Enrichment of Lymphocytes for Use in Adoptive Immunotherapy Using a Modified Counterflow Centrifugal Elutriation Program. *Cytotherapy* **2009**, *11*, 923–935.

13. TerumoBCT. ELUTRA Cell Separation System: Manufacturer Recommendations for the Enrichment of Lymphocytes from Apheresis. http://img03.en25.com/Web/TerumoBCT/%7B92a7e99a-48ef-4272-9422-a5b5b45d3d18%7D_306510006B_Elutra_Enrichment_of_Lymphocytes.pdf?elq=594e474e90b64b4ba335203596d07a24&elqaid=207&elqat=1&elqTrackId=2e7904b17d05445caad44a9970c1d715.

14. Chiche-Lapierre, C. E.; Tramalloni, D.; Chaput, N.; et al. Comparative Analysis of Sepax S-100, COBE 2991, and Manual DMSO Removal Techniques from Cryopreserved Hematopoietic Stem Cell Apheresis Product. *Cytotherapy* **2016**, *18*, 6:S47.

15. Yousuff, C. M.; Wei Ho, E. T.; Hussein, K. I.; et al. Microfluidic Platform for Cell Isolation and Manipulation Based on Cell Properties. *Micromachines* **2017**, *8*, 15.

16. Warkiani, M. E.; Wu, L.; Ping Tay, A. K.; et al. Large Volume Microfluidic Cell Sorting for Biomedical Applications. *Ann. Rev. Biomed. Eng.* **2015**, *17*, 1–34.

17. Huang, L.; Cox, E.; Austin, R. Continuous Particle Separation through Deterministic Lateral Displacement. *Science* **2004**, *304*, 987–990.

18. Davis, J. A.; Inglis, D. W.; Morton, K. J.; et al. Deterministic Hydrodynamics: Taking Blood Apart. *Proc. Natl. Acad. Sci. USA* **2006**, *103*, 14779–14784.

19. Inglis, D. W.; Davis, J. A.; Austin, R. H. Critical Particle Size for Fractionation by Deterministic Lateral Displacement. *Lab Chip* **2006**, *6*, 655–658.

20. Chen, Y.; D'Silva, J.; Austin, R.; et al. Microfluidic Chemical Processing with On-Chip Washing by Deterministic Lateral Displacement Arrays with Separator Walls. *Biomicrofluidics* **2015**, *9*(5), 054105.

21. Shilun, F.; Skelley, A.; Anwer, A. G.; et al. Maximizing Particle Concentration in Deterministic Lateral Displacement Arrays. *Biomicrofluidics* **2017**, *11*, 024121.

22. D'Silva, J. *Throughout Microfluidic Capture of Rare Cells from Large Volumes of Blood*. PhD Dissertation, Princeton University, 2016.

23. Li, Y.; Kurlander, R. J. Comparison of Anti-CD3 and Anti-CD28-Coated Beads with Soluble Anti-CD3 for Expanding Human T Cells: Differing Impact on CD8 T Cell Phenotype and Responsiveness to Restimulation. *J. Trans. Med.* **2010**, *8*, 104.

24. Civin, C. I.; Ward, T.; Skelley, A. M.; et al. Automated Leukocyte Processing by Microfluidic Deterministic Lateral Displacement. *Cytometry A* **2016**, *89*, 1073–1083.

25. Reichert, T.; DeBruyere, M.; Deneys, V.; et al. Lymphocyte Subset Reference in Adult Caucasians. *Clin. Immunol. Immunopath*. **1991**, 190–208.

26. National Institute of Standards and Technology (NIST). *NIST/ SEMATECH e-Handbook of Statistical Methods*. August 2017. http://www.itl.nist.gov/div898/handbook.

27. Mahnke, Y. D.; Brodie, T. M.; Sallusto, F.; et al. The Who's Who of T-Cell Differentiation: Human Memory T-Cell Subsets. *Eur. J. Immunol*. **2013**, *43*, 2797–2809.

28. Agrawal, S.; Ganguly, S.; Hjian, P.; et al. PDGF Upregulates CLEC-2 to Induce T Regulatory Cells. *Oncotarget*. **2015**, *6*, 28621–28632.

29. Zhu, L.; Huang, Z.; Stålesen, R.; et al. Platelets Provoke Distinct Dynamics of Immune Response by Differentially Regulating CD4$^+$ T-Cell Proliferation. *J. Throm. Haem*. **2014**, *12*, 1156–1165.

30. Koesdjojo, M.; Lee, Z.; Dosier, C.; et al. DLD Microfluidic Purification and Characterization of Intact and Viable Circulating Tumor Cells in Peripheral Blood. *AACR Annual Meeting* **2016**, abstr. 3956: http://cancerres.aacrjournals.org/content/76/14_Supplement/3956.

31. Loutherback, K. Microfluidic Devices for High Throughput Cell Sorting and Chemical Treatment. PhD dissertation, Princeton University, **2011**.